Effects of cell geometry on reversible vesicular transport

2017 J. Phys. A: Math. Theor. 50 055601

(http://iopscience.iop.org/1751-8121/50/5/055601)

IOP Publishing Journal of Physics A: Mathematical and Theoretical

J. Phys. A: Math. Theor. **50** (2017) 055601 (25pp) doi:10.1088/1751-8121/aa5304

Effects of cell geometry on reversible vesicular transport

Bhargav R Karamched and Paul C Bressloff

Department of Mathematics, University of Utah, 155 South 1400 East, Salt Lake City, UT 84112, USA

E-mail: karamche@math.utah.edu and bressloff@math.utah.edu

Received 13 September 2016, revised 5 December 2016
Accepted for publication 9 December 2016
Published 6 January 2017

Abstract

A major question in cell biology concerns the biophysical mechanism underlying delivery of newly synthesized macromolecules to specific targets within a cell. A recent modeling paper investigated this phenomenon in the context of vesicular delivery to *en passant* synapses in neurons (Bressloff and Levien 2015 *Phys. Rev. Lett.*). It was shown how reversibility in vesicular delivery to synapses could play a crucial role in achieving uniformity in the distribution of resources throughout an axon, which is consistent with experimental observations in *C. elegans* and *Drosophila*. In this work we generalize the previous model by investigating steady-state vesicular distributions on a Cayley tree, a disk, and a sphere. We show that for irreversible transport on a tree, branching increases the rate of decay of the steady-state distribution of vesicles. On the other hand, the steady-state profiles for reversible transport are similar to the 1D case. In the case of higher-dimensional geometries, we consider two distinct types of radially-symmetric microtubular network: (i) a continuum and (ii) a discrete set. In the continuum case, we model the motor-cargo dynamics using a phenomenologically-based advection-diffusion equation in polar (2D) and spherical (3D) coordinates. On the other-hand, in the discrete case, we derive the population model from a stochastic model of a single motor switching between ballistic motion and diffusion. For all of the geometries we find that reversibility in vesicular delivery to target sites allows for a more uniform distribution of vesicles, provided that cargo-carrying motors are not significantly slowed by their cargo. In each case we characterize the loss of uniformity as a function of the dispersion in velocities.

Keywords: intracellular transport, molecular motors, advection-diffusion, Cayley tree

(Some figures may appear in colour only in the online journal)

1. Introduction

A central question in cell biology concerns the mechanisms underlying the localized delivery of macromolecules to subcellular compartments via motor-driven vesicular transport [3]. Such delivery is necessary, for example, when a neuron requires newly synthesized proteins for the formation of new synapses (synaptogenesis) [24], or when there is restructuring of a cell's cytoskeleton during cell growth, mitosis and polarization [9], or when cellular waste materials are delivered to lysosomes [23]. Intracellular active transport consists of two principle components: microtubules and molecular motors. Microtubules are directionally polarized filaments with biophysically distinguishable $(+)$ ends and $(-)$ ends. The type of polarity at a given end of the microtubule dictates what kind of molecular motor will travel along the microtubule in a given direction. For example, kinesin generally walk in the $(+)$ direction along microtubules, whereas dynein tend to walk in the $(-)$ direction [11]. Motors carry vesicles to specified locations throughout a given cell. The question of *how* this is achieved has been a focus of cell biology in recent years. One possibility is that the cell tags motor cargo with a molecular address that routes cargo to specific locations. However, as far as we are aware, there is no experimental evidence suggesting the existence of such a long-range mechanism. A more likely scenario is that local signaling from an active target enhances the probability of vesicular cargo to that target.

A recent modeling study [4] investigated the active transport and delivery of vesicles across *en passant* synapses in the axons of neurons, based on the following experimental observations in *C. elegans* and *Drosophila* [17, 25]: (i) motor-driven cargo exhibits ballistic anterograde or retrograde motion interspersed with periods of long pauses at presynaptic sites; (ii) the capture of vesicles by synapses during the pauses is reversible, in that vesicular aggregation at a site could be inhibited by signaling molecules resulting in dissociation from the target; (iii) the distribution of resources across synapses is relatively uniform—so-called synaptic democracy. In [4] the transport and delivery of vesicles to synaptic targets was modeled using a one-dimensional (1D) advection-diffusion equation. It was shown that in the case of irreversible cargo delivery, the steady-state vesicle density decays exponentially from the soma, whereas the steady-state density is relatively uniform in the reversible case. This suggests that reversibility in vesicular delivery plays a crucial role in achieving a 'fair' distribution of resources within a cell.

Such a principle appears to hold under more general conditions. For example, the original model of [4] assumed that each motor can carry only one vesicle. Using a modified version of the well-known Becker–Doring equations for aggregation-fragmentation phenomena, the analysis can be extended to the case of motors carrying vesicular aggregates, assuming that only one vesicle can be exchanged with a target at any one time [5]. In [6], we generalized the model of [4] by accounting for exclusion effects between motor-cargo complexes. We treated the axon as a 1D lattice, and represented the motion of motors by a system of ordinary differential equations for the mean occupation number at each site. Using a combination of mean field and adiabatic approximations, we obtained TASEP-like hydrodynamic equations representing the dynamics of motor density in the continuum limit. Again, we found that synaptic democracy is achieved in the reversible delivery case, provided the cargo-carrying motors' speed is not greatly reduced by their cargo.

In this paper, we consider another extension of our previous work, namely, the effects of cell geometry on reversible vesicular transport. We begin by briefly recounting the 1D results found in [4], see section 2. Additionally, we investigate the behavior of the steady state density of vesicles when the velocity of cargo-carrying motors is significantly different from free motors, which was not considered in [4]. We then consider a natural extension of the 1D

analysis, namely a branching network (section 3). A tree is an appropriate domain to study synaptic democracy because it can account for the branched structure that is characteristic of axons and dendrites [21]. We show that in the irreversible case, branching increases the rate of decay of the steady-state distribution of vesicles. On the other hand, the steady-state profiles in the reversible case are similar to the 1D case. Moving away from highly polarized cells such as neurons, most cells (including a neuron's soma) have an approximately 3D spherical shape. There are also examples of cells being treated as two-dimensional disks, particularly in the case of motile eukaryotic cells such as keratocytes [13, 18]. Therefore, we consider models of reversible vesicular transport in the disk and the sphere. We take the source of the motor-cargo complexes to be at the origin, and model the dynamics of the motor densities by differential equations transformed into their polar (2D) and spherical (3D) representations. In contrast to the 1D model, we distinguish between two types of filament distributions: (i) the distribution of microtubules emanating from the origin forms a continuum (section 4); (ii) the set of microtubules emanating from the origin forms a discrete set (section 5). In case (i) we model the motion of motor densities using advection-diffusion equations. We find that for irreversible delivery the steady-state vesicle density decays according to a modified Bessel function, whereas a uniform density can be obtained when delivery is reversible. In case (ii) we derive PDEs for the motor density based on stochastic differential equations (SDEs) for individual motor dynamics in the 2D and 3D domains following along the lines of Lawley *et al* [16]. Throughout the paper we ignore boundary effects away from the source of motor-cargo complexes. In the case of exponentially decaying steady-state densities, this is a reasonable approximation provided that the spatial rate of decay is smaller than the size of the physical domain.

2. Semi-infinite track

Before elucidating our model and results, we briefly present the 1D results found in [4].

2.1. Irreversible delivery

Consider a population of motor-cargo complexes or particles moving on a semi-infinite track, each of which carries a single synaptic vesicle precursor (SVP) to be delivered to a synaptic site. Assume that these particles are injected at the soma ($x = 0$) at a fixed rate J_1 and that the distribution of synaptic sites along the axon is uniform. That is, at any given spatial point x, a particle can deliver its cargo to a synapse at a rate k. Neglecting interactions between particles, the dynamics of the motor-cargo complexes can be captured by the advection-diffusion equation [4]

$$\frac{\partial u}{\partial t} = -v\frac{\partial u}{\partial x} + D\frac{\partial^2 u}{\partial x^2} - ku, x \in (0, \infty), \tag{2.1}$$

where $u(x,t)$ is the particle density along the microtubule track at position x at time t. Note that equation (2.1) can be derived from more detailed biophysical models of motor transport under the assumption that the rates at which motor-cargo complexes switch between different motile states are relatively fast [4, 22]. In particular, the mean speed will depend on the relative times that the complex spends in different anterograde, stationary, and possibly retrograde states, whereas the diffusivity D reflects the underlying stochasticity of the motion. Equation (2.1) is supplemented by the boundary condition at $x = 0$:

$$J(u(0,t)) = J_1, \quad J(u) \equiv vu - D\frac{\partial u}{\partial x}. \tag{2.2}$$

Let $c(x, t)$ denote the concentration of delivered vesicles to the presynaptic sites at x at time t with

$$\frac{\partial c}{\partial t} = ku - \lambda c, \tag{2.3}$$

where λ denotes the degradation rate for vesicles. Note that in the irreversible delivery case, including vesicular degradation is necessary to prevent blowup in the solutions for $c(x,t)$. This consideration is not necessary in the reversible delivery case. The steady state solution for c is given by

$$c = \frac{k}{\lambda}\frac{J_1 e^{-\xi x}}{D\xi + v} \qquad \xi = \frac{-v + \sqrt{v^2 + 4Dk}}{2D}, \tag{2.4}$$

which clearly indicates that c decays exponentially with respect to distance from the soma with correlation length ξ^{-1}. Taking the values $D = 1.0\ \mu\text{m s}^{-1}$ for cytoplasmic diffusion and $v = 0.1 - 1\ \mu\text{m s}^{-1}$ for motor transport [11], and assuming that $k \ll 1\text{s}^{-1}$, we see that $\bar{\xi} \approx (v/k)\ \mu\text{m}$. Thus, in order to have correlation lengths comparable to axonal lengths of several millimeters, we would require delivery rates of the order $k \sim 10^{-5}\ \text{s}^{-1}$, whereas measured rates tend to be of the order of a few per minute [4, 8, 15]. This simple calculation establishes that injecting motor-complexes from the somatic end of the axon leads to an exponentially decaying distribution of synaptic resources along the axon. We now show, following [4], that relaxing the irreversible delivery condition in this model allows for a more uniform distribution of vesicles along the axon.

2.2. Reversible delivery

In order to take into account the reversibility of vesicular delivery to synapses, one must consider a generalization of the advection-diffusion model (2.1). To that end, let $u_0(x,t)$ and $u_1(x,t)$ denote the density of motor-cargo complexes without and with an attached SVP, respectively, and let k_+ and k_- denote the rates at which vesicles are delivered to synaptic sites and recovered by the motors, respectively. Each density evolves according to an advection-diffusion equation combined with transition rates that represent the delivery and recovery of SVPs:

$$\frac{\partial u_0}{\partial t} = -v_0\frac{\partial u_0}{\partial x} + D\frac{\partial^2 u_0}{\partial x^2} - \gamma_0 u_0 + k_+ u_1 - k_- c u_0 \tag{2.5a}$$

$$\frac{\partial u_1}{\partial t} = -v_1\frac{\partial u_1}{\partial x} + D\frac{\partial^2 u_1}{\partial x^2} - \gamma_1 u_1 - k_+ u_1 + k_- c u_0, \tag{2.5b}$$

with $x \in (0, \infty)$. Disparity in the velocities in each state reflects the effect cargo can have on particle motility, whilst the degradation rates $\gamma_{0,1}$ are included to account for the possibility of particle degradation or recycling. Equations (2.5*a*) and (2.5*b*) are supplemented by the boundary conditions

$$J(u_j(0,t)) = J_j, \qquad j = 0, 1, \tag{2.6}$$

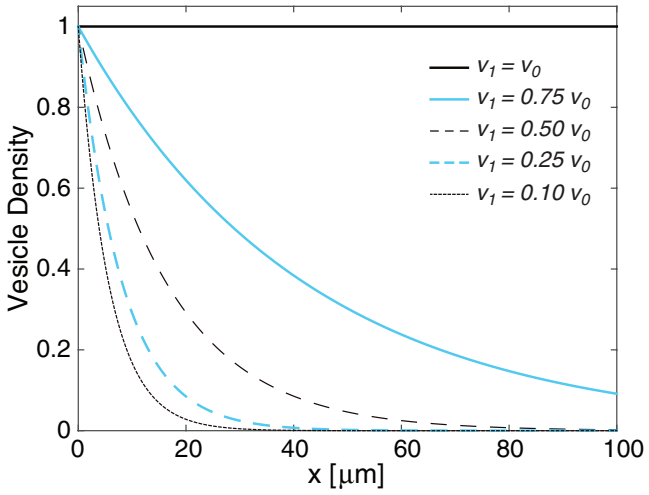

Figure 1. Figure depicting the loss of synaptic democracy as disparity in velocities between free motors and cargo-carrying motors grows normalized so all curves fit in one frame. Parameter values are $D = 0.1\ \mu\text{m}^2\ \text{s}^{-1}$, $\gamma_{0,1} = 0.01\,\text{s}^{-1}$, $k_\pm = 0.01\,\text{s}^{-1}$, $J_0 = J_1$, $v_0 = 0.1\ \mu\text{m s}^{-1}$. Vesicle density is normalized so that $c(0) = 1$.

where J_j is the constant rate at which particles with or without cargo are injected into the axon from the soma. The dynamics for $c(x, t)$ are now given by

$$\frac{\partial c}{\partial t} = k_+ u_1 - k_- c u_0. \tag{2.7}$$

We need not explicitly include degradation in this case because, provided $J_0 > 0$, $c(x, t)$ will be bounded. The steady state distribution of vesicles is then

$$c = \frac{k_+ u_1}{k_- u_0}$$

Substitution into the steady state analogs of equations (2.5*a*) and (2.5*b*) yields

$$u_j(x) = \frac{J_j \mathrm{e}^{-\xi_j x}}{D\xi_j + v_j} \quad \xi_j = \frac{-v_j + \sqrt{v_j^2 + 4D\gamma_j}}{2D} \tag{2.8}$$

whence

$$c = \frac{k_+}{k_-}\frac{J_1}{J_0}\frac{D\xi_0 + v_0}{D\xi_1 + v_1}\mathrm{e}^{-\Gamma x} \tag{2.9}$$

with $\Gamma \equiv \xi_1 - \xi_0$. It is evident that if $\Gamma = 0$, then c has a spatially uniform distribution.

Suppose that the diffusion and degradation rates of motors do not change when carrying cargo. Then $\Gamma = 0$ would imply that the velocities of the cargo-carrying motors are equal to the velocities of the free motors. However, we would expect $v_1 < v_0$ due to the added load of the cargo on the motor, and that this would lead to a loss of synaptic democracy since $\Gamma > 0$. Indeed, values of v_1 less than v_0 lead to steady state profiles of vesicle density reminiscent of the exponential decay behavior of the irreversible delivery case, see figure 1, although the spatial rate of decay is mitigated by the presence of reversible delivery. Hence, attaining synaptic democracy also depends on physical properties of the cargo being carried. Large cargo, for example, may not be uniformly distributed throughout an axon whereas smaller cargo will.

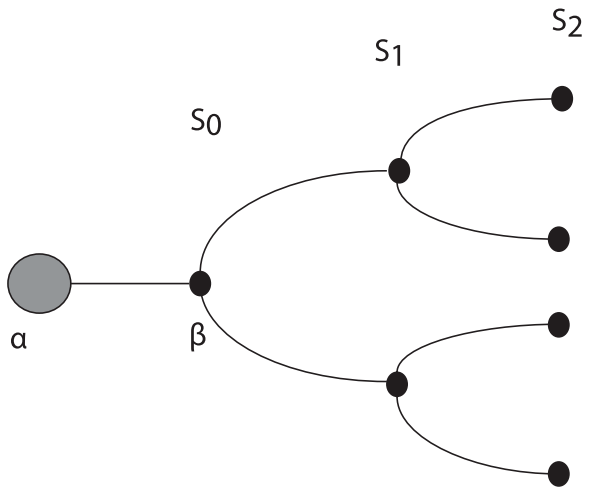

Figure 2. Cayley tree Λ with $z = 2$.

3. Cayley tree

One limitation of the above model is that it does not capture the highly branched nature of an axon. Therefore, we now investigate irreversible and reversible delivery of vesicles to synapses on a tree. For simplicity, we consider an unbounded, regular tree Λ radiating from a unique origin with branching number z and segment length L (a Cayley tree), see figure 2. We denote the origin, or the mother node, by α and the tree node opposite of the mother node by β. Let S_1 be the set of z downstream nodes connected to β. Similarly, let S_2 consist of the z^2 downstream nodes that are connected to the vertices of the first generation and so on. The nth generation thus consists of z^n nodes. Since all nodes (and their associated branches) of a given generation are equivalent for a regular tree, we can consider a single direct path through the tree and label the branch linking the node in S_{i-1} to the node in S_i by i, $i = 0, 1, 2, \ldots$, where S_0, S_{-1} are identified with the nodes β and α, respectively.

Consider a population of motor-cargo complexes or particles moving on Λ, each of which carries a single synaptic vesicle precursor (SVP) to be delivered to a synaptic site. Motors are injected into the tree at a constant rate J_1 at the mother node, α. Each branch is of finite length L, and we denote the point on each branch closest to α as $x = 0$ and the point farthest away from α by $x = L$. The movement of the motors along a branch preceding a node in S_i can be modeled by an advection-diffusion equation

$$\frac{\partial u_i}{\partial t} = -v\frac{\partial u_i}{\partial x} + D\frac{\partial^2 u_i}{\partial x^2}, \tag{3.1}$$

where $u_i(x, t)$ represents the motor density at position x at time t, D is the motor diffusion coefficient, and v is the motor velocity. In the following, equation (3.1) will be coupled with the boundary conditions

$$\begin{aligned} u_i(L,t) &= u_{i+1}(0,t) \quad i \geqslant 0 \\ J_0(0,t) &= J_1 \\ J_i(L,t) &= zJ_{i+1}(0,t), \quad i \geqslant 1. \end{aligned} \tag{3.2}$$

The first boundary condition represents continuity of motor density at the nodes of the tree. The second boundary condition represents the constant injection rate of motors at the

mother node, and the last boundary condition reflects Kirchoff's law of conservation of current. Here,

$$J_i(x,t) = vu_i - D\frac{\partial u_i}{\partial x}$$

Note that for simplicity we take the motor velocity and diffusivities to be the same in all branches of the tree. A more detailed model would need to take into account a number of features. For example, exclusion effects could mean motor velocities are locally density dependent, and diffusivities could change if the cross-sectional area of the axon decreases along the tree. Let us now use this setup to investigate irreversible and reversible vesicular delivery, respectively, to target synapses.

3.1. Irreversible delivery

We modify equation (3.1) by including a degradation term to account for irreversible delivery of vesicles. Let $c_i(x, t)$ denote the concentration of vesicles at position x at time t on the ith branch. The model for motor and vesicle dynamics is given by

$$\frac{\partial u_i}{\partial t} = -v\frac{\partial u_i}{\partial x} + D\frac{\partial^2 u_i}{\partial x^2} - ku_i \tag{3.3a}$$

$$\frac{\partial c_i}{\partial t} = ku_i - \lambda c_i, \tag{3.3b}$$

where λ is the vesicular degradation rate. At steady state we have

$$-v\frac{\partial u_i}{\partial x} + D\frac{\partial^2 u_i}{\partial x^2} - ku_i = 0 \tag{3.4a}$$

$$c = \frac{ku_i}{\lambda} \tag{3.4b}$$

The general solution to equation (3.4*a*) is given by

$$u_i(x) = A_i e^{\xi_+ x} + B_i e^{\xi_- x}, \qquad \xi_\pm \equiv \frac{v \pm \sqrt{v^2 + 4Dk}}{2D}, \tag{3.5}$$

where A_i, B_i are constants of integration to be determined from boundary conditions. We can determine one of the constants for u_0 by imposing the boundary condition reflecting the injection rate of motors. For the remaining constants, we employ the following method. We assume the motor density at each node in S_i is given by Φ_{i+1}. This ensures the solution on the tree will be continuous at the nodes. We then impose the boundary condition reflecting Kirchoff's law to determine each value Φ_i. That is, assume

$$u_0(0) = \Phi_0 \tag{3.6a}$$

$$u_0(L) = u_1(0) = \Phi_1 \tag{3.6b}$$

$$u_{i-1}(L) = u_i(0) = \Phi_i, \quad i \geqslant 2 \tag{3.6c}$$

From equations (3.5) and (3.6*c*) we have for $i \geqslant 1$

$$u_i(x) = \frac{\Phi_i e^{\xi_- L} - \Phi_{i+1}}{e^{\xi_- L} - e^{\xi_+ L}} e^{\xi_+ x} + \frac{\Phi_{i+1} - \Phi_i e^{\xi_+ L}}{e^{\xi_- L} - e^{\xi_+ L}} e^{\xi_- x} \tag{3.7}$$

Imposing the current conservation condition (3.2), we obtain the following linear homogenous recurrence relation:

$$z(\xi_+ - \xi_-)\Phi_{i+1} + (\xi_+ - \xi_-)e^{(\xi_+ + \xi_-)L}\Phi_{i-1} + \left(\frac{v(z-1)(e^{\xi_- L} - e^{\xi_+ L})}{D} + \xi_-(e^{\xi_- L} + z e^{\xi_+ L}) - \xi_+(e^{\xi_+ L} + z e^{\xi_- L}) \right)\Phi_i = 0. \tag{3.8}$$

Equation (3.8) has the solution $\Phi_i = \nu^i$ with ν determined from the characteristic equation

$$z(\xi_+ - \xi_-)\,\nu^2 + \left(\frac{v(z-1)(e^{\xi_- L} - e^{\xi_+ L})}{D} + \xi_-(e^{\xi_- L} + z e^{\xi_+ L}) - \xi_+(e^{\xi_+ L} + z e^{\xi_- L}) \right)\nu + (\xi_+ - \xi_-)e^{(\xi_+ + \xi_-)L} = 0. \tag{3.9}$$

We obtain two solutions $\nu_\pm$ in solving the quadratic equation, with $|\nu_+| > 1$ and $|\nu_-| < 1$. Hence,

$$\Phi_i = c_1 \nu_+^i + c_2 \nu_-^i. \tag{3.10}$$

In the case of an unbounded tree we set $c_1 = 0$, otherwise $|\Phi_n| \to \infty$ as $n \to \infty$. Hence, we have $\Phi_i = c\nu_-^i$. Setting $i = 0$ gives $c = \Phi_0$. Hence,

$$\Phi_i = \Phi_0 \nu_-^i \tag{3.11}$$

It remains to determine Φ_0. First, imposing the boundary conditions $u_0(L) = \Phi_1$ and $J_0(0) = J_1$, the solution for $u_0(x)$ is given by

$$u_0(x) = \frac{J_1 e^{\xi_- L} - (v - D\xi_-)\Phi_1}{[v - D\xi_+]e^{\xi_- L} - [v - D\xi_+]e^{\xi_- L}} e^{\xi_+ x} + \frac{(v - D\xi_+)\Phi_1 - J_1 e^{\xi_+ L}}{[v - D\xi_+]e^{\xi_- L} - [v - D\xi_-]e^{\xi_+ L}} e^{\xi_- x}. \tag{3.12}$$

From equation (3.11), we obtain that $\Phi_1 = \Phi_0 \nu_-$. On the other hand, by substituting $x = 0$ into equation (3.12), we obtain

$$\Phi_1 = \frac{\Phi_0([v - D\xi_+]e^{\xi_- L} - [v - D\xi_-]e^{\xi_+ L}) - J_1(e^{\xi_- L} - e^{\xi_+ L})}{D(\xi_- - \xi_+)}$$

Equating the above two equations for Φ_1 gives the explicit formula for Φ_0,

$$\Phi_0 = -J_1 \frac{e^{\xi_- L} - e^{\xi_+ L}}{D\nu_-(\xi_- - \xi_+) - ([v - D\xi_+]e^{\xi_- L} - [v - D\xi_-]e^{\xi_+ L})} \tag{3.13}$$

We can now use equation (3.11) to obtain $\Phi_i, \forall\, i \in \Lambda$. Hence, we have the steady state distribution of vesicles in the Cayley tree in the irreversible delivery case.

In figure 3 we compare the decay of vesicle density in the irreversible case of the Cayley tree to the semi-infinite track. We can see that toward the soma, the profiles are in exact agreement, whereas as soon as we reach the first branching point of the tree, the steady state vesicle density suddenly drops, thereby aggravating the decay in the case of the Cayley tree to be

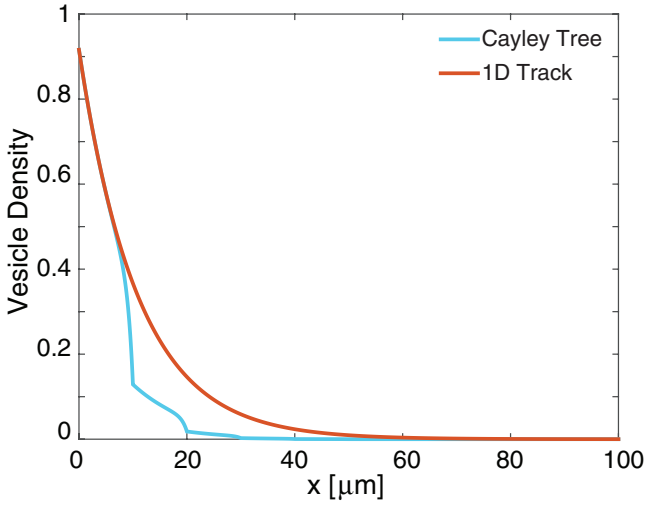

Figure 3. Plot comparing steady state vesicle densities in the irreversible delivery case of the semi-infinite track and the Cayley tree. Parameter values are $L = 10$ μm, $v = 0.1$ μm s^{-1}, $D = 0.1$ μm^2 s^{-1}, $z = 3$, $\lambda = k = 0.01\,\mathrm{s}^{-1}$. Vesicle density is normalized so that $c(0) = 1$.

greater than in the semi-infinite track. This suggests that if vesicular delivery were irreversible, biased delivery toward the soma would be greater than predicted in [4].

3.2. Reversible delivery

To allow for re-uptake of vesicles from target sites, we must include the dynamics of cargo-carrying motors, $u_1^i(x,t)$ as well as free motors, $u_0^i(x,t)$, on each branch i and add switching terms to the advection diffusion equation (3.1). Let $c^i(x,\,t)$ represent the density of vesicles at position x at time t on branch i, $i \in S_n$. Then the motor and vesicle dynamics are given by

$$\frac{\partial u_0^i}{\partial t} = -v_0\frac{\partial u_0^i}{\partial x} + D\frac{\partial^2 u_0^i}{\partial x^2} - \gamma_0 u_0^i + k_+ u_1^i - k_- c^i u_0^i \tag{3.14a}$$

$$\frac{\partial u_1^i}{\partial t} = -v_1\frac{\partial u_1^i}{\partial x} + D\frac{\partial^2 u_1^i}{\partial x^2} - \gamma_1 u_1^i - k_+ u_1^i + k_- c^i u_0^i \tag{3.14b}$$

$$\frac{\partial c^i}{\partial t} = k_+ u_1^i - k_- c^i u_0^i. \tag{3.14c}$$

We couple equations (3.14*a*) and (3.14*b*) with the boundary conditions (3.2). Let $J_{0,1}$ be the injection rates at the origin for $u_{0,1}$, respectively. At steady state, we have

$$D\frac{\partial^2 u_0^i}{\partial x^2} - v_0\frac{\partial u_0^i}{\partial x} - \gamma_0 u_0^i = 0 \tag{3.15a}$$

$$D\frac{\partial^2 u_1^i}{\partial x^2} - v_1\frac{\partial u_1^i}{\partial x} - \gamma_1 u_1^i = 0 \tag{3.15b}$$

$$c^i = \frac{k_+ u_1^i}{k_- u_0^i}. \tag{3.15c}$$

As equations (3.15*a*) and (3.15*b*) are decoupled, we may apply the method elaborated in the irreversible delivery case to each equation separately and then obtain the full solution on the Cayley Tree. For example, let

$$\begin{aligned} &u_0^0(0) = \Phi_0 && u_1^0(0) = \Psi_0 \\ &u_0^0(L) = u_0^1(0) = \Phi_1 && u_1^0(L) = u_1^1(0) = \Psi_1 \\ &u_0^{i-1}(L) = u_0^i(0) = \Phi_i && u_1^{i-1}(L) = u_1^i(0) = \Psi_i. \end{aligned}$$

so that the solutions are continuous at all nodes of Λ. We then have for $i \geqslant 1$

$$u_0^i(x) = \frac{\Phi_i e^{\xi_- L} - \Phi_{i+1}}{e^{\xi_- L} - e^{\xi_+ L}} e^{\xi_+ x} + \frac{\Phi_{i+1} - \Phi_i e^{\xi_+ L}}{e^{\xi_- L} - e^{\xi_+ L}} e^{\xi_- x} \tag{3.16a}$$

$$u_1^i(x) = \frac{\Psi_i e^{\zeta_- L} - \Psi_{i+1}}{e^{\zeta_- L} - e^{\zeta_+ L}} e^{\zeta_+ x} + \frac{\Psi_{i+1} - \Psi_i e^{\zeta_+ L}}{e^{\zeta_- L} - e^{\zeta_+ L}} e^{\zeta_- x}, \tag{3.16b}$$

with

$$\xi_\pm \equiv \frac{v_0 \pm \sqrt{v_0^2 + 4D\gamma_0}}{2D} \qquad \zeta_\pm \equiv \frac{v_1 \pm \sqrt{v_1^2 + 4D\gamma_1}}{2D}$$

By imposing conservation of current at each node, we obtain second-order iterative equations for Φ_i and Ψ_i, which can be solved to give

$$\Phi_i = \nu_-^i \Phi_0, \quad \Psi_i = \mu_-^i \Psi_0,$$

where ν_- is the smaller root of equation (3.9) and μ_- is the smaller root of the corresponding quadratic equation obtained by the replacement $\xi_\pm \to \zeta_\pm$. Finally, solving the equations for $u_0^0(x)$ and $u_1^0(x)$ and imposing the boundary conditions $u_0^0(L) = \Phi_1, u_1^0(L) = \Psi_1$ yields

$$\Phi_0 = -\frac{J_0}{D} \frac{e^{\xi_- L} - e^{\xi_+ L}}{\nu_-(\xi_- - \xi_+) - (\xi_- e^{\xi_- L} - \xi_+ e^{\xi_+ L})}. \tag{3.17}$$

and

$$\Psi_0 = -\frac{J_1}{D} \frac{e^{\zeta_- L} - e^{\zeta_+ L}}{\nu_-(\zeta_- - \zeta_+) - (\zeta_- e^{\zeta_- L} - \zeta_+ e^{\zeta_+ L})}. \tag{3.18}$$

Thus, we obtain the steady-state vesicle distribution. Note that if $\gamma_0 = \gamma_1$, then $\xi_\pm = \zeta_\pm$ when $v_0 = v_1$ and $u_1^i(x) = u_0^i(x)$ for all $x \in [0, L]$ and $i \geqslant 0$. It follows that the vesicle distribution is uniform.

In figure 4, we show how uniformity in vesicle distribution is lost when $v_1 < v_0$ and compare decays in the Cayley tree with $z = 3$, $L = 1$ to decays on the semi-infinite track. We can see that the steady state profiles are similar. Interestingly, the tree domain seems to facilitate a higher density of vesicles farther along in the domain than the semi-infinite track. We now investigate the impact of reversible vesicle delivery in higher dimensional domains.

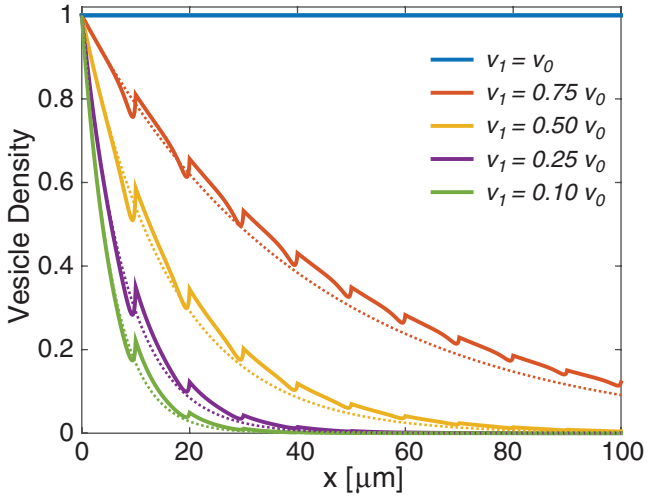

Figure 4. Plots showing loss of vesicular uniformity as v_1 decreases in the case of a Cayley tree (kinked curves) and a semi-infinite track (smooth dotted curves). Parameter values are $v_0 = 0.1\ \mu\text{m s}^{-1}$, $D = 0.1\ \mu\text{m s}^{-1}$, $\gamma_{0,1} = 0.01\,\text{s}^{-1}$, $k_\pm = 0.01\,\text{s}^{-1}$, $L = 10\ \mu\text{m}$, $z = 3$, $J_0 = J_1$. Vesicle density is normalized so that $c(0) = 1$.

4. Higher-dimensional geometries

Although a 1D model is a reasonable first approximation of microtubule-based active transport in the axons and dendrites of a highly polarized cell such as a neuron, in most cells intracellular transport takes place along 2D or 3D cytoskeletal networks of microtubules. For a sufficiently dense network one could imagine carrying out some form of homogenization to obtain a continuum of microtubules. On the other hand, for a sparse network, the discrete nature of microtubules has to be taken into account. Here we focus on the continuum case; discrete microtubular networks will be considered in section 5. For simplicity, we model a cell as a disk or a sphere and assume that the density of microtubules is radially symmetric, that is, we ignore the curvature of microtubules. We take the source of the motor-cargo complexes to be at the origin of the cell, and represent the dynamics of the motor densities by advection-diffusion equations transformed into their polar (2D) and spherical (3D) representations. We will also assume that each motor carries one cargo element and can deliver its cargo at any point within the given domain. In other words, we assume that there is a continuum of target sites within the cell.

4.1. The disk

Let $\Omega_2 \equiv \mathbb{R}^2 \setminus B_\delta(\mathbf{0})$, where $B_\delta(\mathbf{0})$ is the disk of radius δ centered at the origin, with $0 < \delta \ll 1$. In polar coordinates

$$\Omega_2 = \{(r,\theta) | r \geqslant \delta,\ 0 \leqslant \theta \leqslant 2\pi\}.$$

We model the dynamics of the motor population by an advection-diffusion equation that is a radially symmetric 2D analog of the 1D model. As in the previous cases, we first consider irreversible vesicle delivery and then reversible vesicle delivery.

4.1.1. Irreversible delivery. Let $u(r, t)$ and $c(r, t)$ denote, respectively, the density of motors and vesicles at a radial distance r from the origin at time t. The motor and vesicle densities are taken to evolve according to the equations

$$\frac{\partial u}{\partial t} = D\frac{\partial^2 u}{\partial r^2} + \frac{D-\mathcal{V}}{r}\frac{\partial u}{\partial r} - ku \tag{4.1a}$$

$$\frac{\partial c}{\partial t} = ku - \lambda c \tag{4.1b}$$

where D is the diffusion coefficient, $v = \mathcal{V}/r$ is a divergence-free motor velocity[1], and λ is the degradation rate of vesicles. As in the 1D case, we model irreversible vesicle delivery using an effective degradation term in equation (4.1*a*). We pair equation (4.1*a*) with the boundary conditions

$$u(\delta) = u_0 \qquad \lim_{r\to\infty} u(r) = 0, \tag{4.2}$$

where $u_0 > 0$ denotes the density of motors on $\partial B_\delta(0)$. At steady state, we have the equations

$$D\frac{\partial^2 u}{\partial r^2} + \frac{D-\mathcal{V}}{r}\frac{\partial u}{\partial r} - ku = 0 \tag{4.3a}$$

$$c = \frac{ku}{\lambda} \tag{4.3b}$$

The steady state vesicle density profile is immediately given by a modified Bessel function of the second kind:

$$c(r) = \frac{ku_0}{\lambda}\frac{r^{\frac{\nu}{2D}}K_{\frac{\nu}{2D}}\left(\frac{r}{\sqrt{D/k}}\right)}{\delta^{\frac{\nu}{2D}}K_{\frac{\nu}{2D}}\left(\frac{\delta}{\sqrt{D/k}}\right)} \tag{4.4}$$

As in previous geometries, irreversible vesicular delivery results in a decaying steady state profile for vesicle density. In figure 5, we compare the decay in the disk with the decay on the semi-infinite track. We can see that towards the origin the Bessel function distributes vesicles more liberally than the exponential function but then rapidly decays below the latter. We also show a plot of the corresponding decay in the case of a sphere (see section 4.2), which is similar to the disk. Let us now look at the reversible vesicle delivery case.

4.1.2. Reversible delivery. To account for the possibility of re-uptake of vesicles by free motors, we model the dynamics of both the free motor density, $u_0(r, t)$, and the cargo-carrying motor density, $u_1(r, t)$. We thus have a pair of radially symmetric advection-diffusion equations coupled with switching terms that reflect vesicle delivery and uptake. Again, let $c(r, t)$ denote the vesicle density at a distance r from the origin at time t. The system of equations is

$$\frac{\partial u_0}{\partial t} = D\frac{\partial^2 u_0}{\partial r^2} + \frac{D}{r}\frac{\partial u_0}{\partial r} - \frac{\mathcal{V}_0}{r}\frac{\partial u_0}{\partial r} - \gamma_0 u_0 - k_+ c u_0 + k_- u_1 \tag{4.5a}$$

$$\frac{\partial u_1}{\partial t} = D\frac{\partial^2 u_1}{\partial r^2} + \frac{D}{r}\frac{\partial u_1}{\partial r} - \frac{\mathcal{V}_1}{r}\frac{\partial u_1}{\partial r} - \gamma_1 u_1 + k_+ c u_0 - k_- u_1 \tag{4.5b}$$

[1] This is motivated by the idea that the density of microtubules decreases as r^{-1} in the 2D case (and decreases as r^{-2} in the 3D case). When we consider a discrete distribution of microtubules the effective velocity will have a more complicated r-dependence.

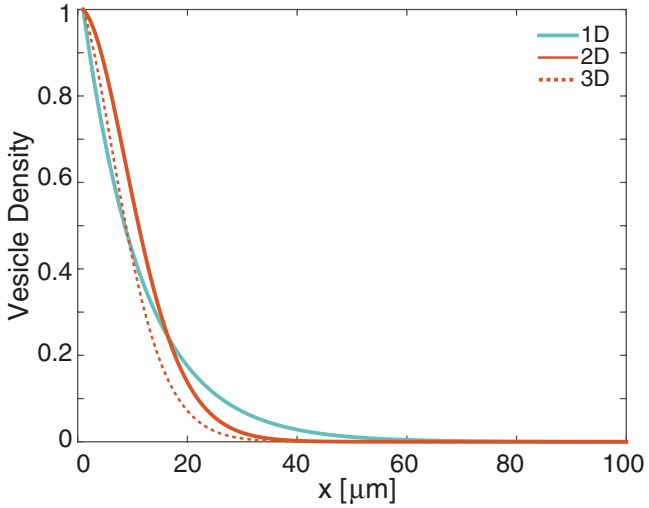

Figure 5. Figure comparing irreversible vesicular profiles from equations (4.4) and (2.4). Here x either represents 1D distance or a radial coordinate. Parameter values are $D = 0.1\ \mu\text{m}^2\,\text{s}^{-1}, \mathcal{V} = 1\,\mu\text{m}^2\,\text{s}^{-1}, \lambda = k = 0.01\,\text{s}^{-1}, \delta = 0.1\,\mu\text{m}$, and the flux J_1 is chosen appropriately so as to match up left boundary data. Also shown is the corresponding steady-state density for the sphere. Vesicle density is normalized so that $c(0) = 1$.

$$\frac{\partial c}{\partial t} = -k_+ c u_0 + k_- u_1, \tag{4.5c}$$

where D is the motor diffusion coefficient, $v_{0,1} = \mathcal{V}_{0,1}/r$ are divergence-free velocities of the free and cargo-carrying motors, respectively, $k_\pm$ denote the rates of vesicle uptake and delivery, respectively, and $\gamma_{0,1}$ are motor degradation rates. We again point out that the reversibility in vesicle delivery means that we do not need to include a degradation term in equation (4.5c). The corresponding system at steady state is

$$D\frac{\partial^2 u_0}{\partial r^2} + \frac{D}{r}\frac{\partial u_0}{\partial r} - \frac{\mathcal{V}_0}{r}\frac{\partial u_0}{\partial r} - \gamma_0 u_0 = 0 \tag{4.6a}$$

$$D\frac{\partial^2 u_1}{\partial r^2} + \frac{D}{r}\frac{\partial u_1}{\partial r} - \frac{\mathcal{V}_1}{r}\frac{\partial u_1}{\partial r} - \gamma_1 u_1 = 0 \tag{4.6b}$$

$$c = \frac{k_- u_1}{k_+ u_0}, \tag{4.6c}$$

The solution for $u_l(r, t)$, $l = 0,1$, is

$$u_l = u_l^0 \frac{r^{\frac{\mathcal{V}_l}{2D}} K_{\frac{\mathcal{V}_l}{2D}}\left(\sqrt{\frac{\gamma_l}{D}}\, r\right)}{\delta^{\frac{\mathcal{V}_l}{D}} K_{\frac{\mathcal{V}_l}{2D}}\left(\sqrt{\frac{\gamma_l}{D}}\,\delta\right)},$$

where u_l^0 denotes the boundary data at the origin for u_l. It immediately follows that

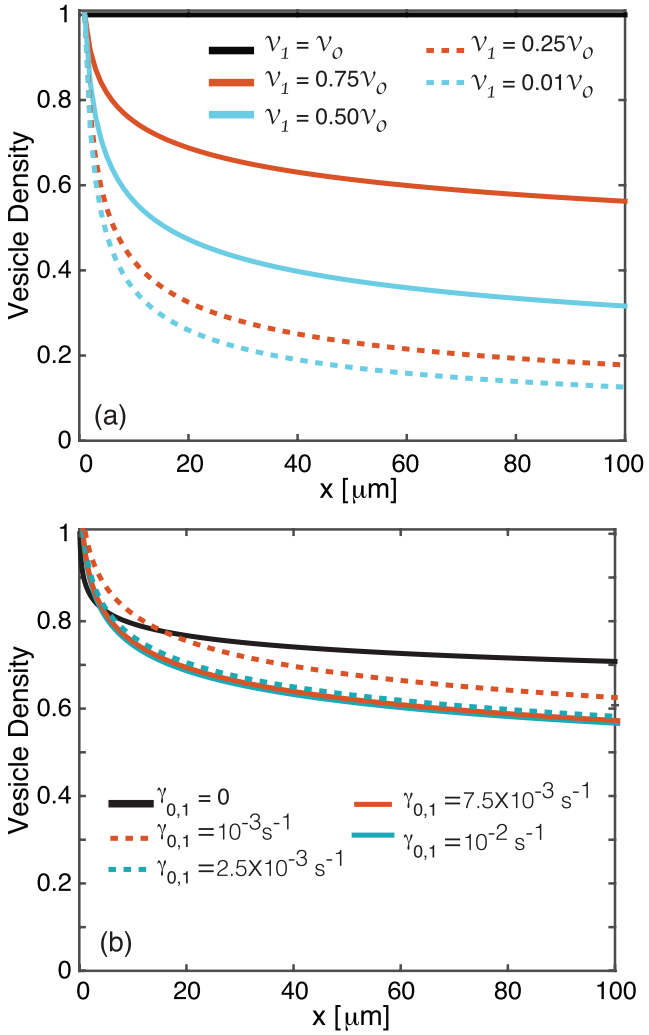

Figure 6. Figure showing loss of vesicular uniformity on the disk as $\mathcal{V}_1$ decreases. (a) Plot of steady-state vesicle density for various $\mathcal{V}_1$ values and fixed motor degradation rates $\gamma_{0,1} = 0.01\ s^{-1}$. (b) Corresponding plots for various degradation rates and $\mathcal{V}_1 = 7.5\ \mu m^2\ s^{-1}$. Other parameter values are $\mathcal{V}_0 = 1\ \mu m^2\ s^{-1}$, $D = 0.1\ \mu m^2\ s^{-1}$, $\delta = 0.1\,\mu m$, $k_\pm = 0.011\,s^{-1}$, $\gamma_{0,1} = 0.10\,s^{-1}$, $u_0^0 = u_1^0$.

$$c = \frac{k_-}{k_+}\frac{u_1^0}{u_0^0}\left(\frac{r}{\delta}\right)^{\frac{\mathcal{V}_1-\mathcal{V}_0}{2D}}\frac{K_{\frac{\mathcal{V}_0}{2D}}\left(\sqrt{\frac{\gamma_0}{D}}\,\delta\right)}{K_{\frac{\mathcal{V}_1}{2D}}\left(\sqrt{\frac{\gamma_1}{D}}\,\delta\right)}\frac{K_{\frac{\mathcal{V}_1}{2D}}\left(\sqrt{\frac{\gamma_1}{D}}\,r\right)}{K_{\frac{\mathcal{V}_0}{2D}}\left(\sqrt{\frac{\gamma_0}{D}}\,r\right)}. \tag{4.7}$$

Suppose that the motor degradation rates are equal, $\gamma_1 = \gamma_0$. It is clear that if $\mathcal{V}_1 = \mathcal{V}_0$, then the vesicle distribution is uniform. On the other hand, we find that if $\mathcal{V}_1 < \mathcal{V}_0$, then the spatial profile is a decaying function of r, see figure 6(a). The behavior here is consistent with what is seen along

the semi-infinite track, although in the latter case the decay is exponential. As expected the rate of decay is mitigated by a reduction in the motor degradation rates as shown in figure 6(b).

4.2. The sphere

Let $\Omega_3 \equiv \mathbb{R}^3 \setminus B_\delta(\mathbf{0})$, where $B_\delta(\mathbf{0})$ is the ball of radius δ centered at the origin, with $0 < \delta \ll 1$. In spherical coordinates, the domain is defined as

$$\Omega_3 = \{(\rho, \theta, \phi) | \rho \geqslant \delta,\ 0 \leqslant \theta \leqslant 2\pi,\ 0 \leqslant \phi \leqslant \pi\}.$$

As in the case of a disk, we consider a population of motors sourced at the origin switching between diffusive and ballistic transport, depending on whether or not a given motor is bound to a microtubule. The dynamics of the motor population is modeled by a radially-symmetric 3D advection-diffusion equation analogous to the 1D model. Let $u(\rho, t)$ denote the density of motors located at a radial distance r from the origin at time t.

4.2.1. Irreversible delivery. Let $c(\rho, t)$ represent the density of vesicles at a distance of ρ from the origin at time t. Then the dynamics of the motor and vesicle densities are given by

$$\frac{\partial u}{\partial t} = D\frac{\partial^2 u}{\partial \rho^2} + \left(\frac{2D}{\rho} - \frac{\mathcal{V}}{\rho^2}\right)\frac{\partial u}{\partial \rho} - ku \tag{4.8a}$$

$$\frac{\partial c}{\partial t} = ku - \lambda c, \tag{4.8b}$$

where D is the motor diffusion coefficient, $\mathcal{V}/\rho^2$ is a divergence-free motor velocity, and λ is the vesicular degradation rate. As in the previous analysis, vesicular degradation must be accounted for in the irreversible delivery case to ensure vesicle profiles do not blow up. It is not necessary in the reversible case. We pair equation (4.8*a*) with the boundary conditions

$$u(\delta) = u_0 \qquad \lim_{\rho \to \infty} u(\rho) = 0,$$

where $u_0 > 0$ is the density of motors on ∂B. At steady state, we have the system

$$D\frac{\partial^2 u}{\partial \rho^2} + \left(\frac{2D}{\rho} - \frac{\mathcal{V}}{\rho^2}\right)\frac{\partial u}{\partial \rho} - ku = 0$$
$$c = \frac{ku}{\lambda}.$$

As the steady state equations are difficult to solve analytically, we solve them numerically. In figure 5, we compare the decay of the steady-state vesicle density in 3D with the 1D and 2D domains. We find that the 3D steady state profile behaves similarly to the 2D case.

4.2.2. Reversible delivery. In the reversible delivery case, we keep track of the free motor densities, $u_0(\rho, t)$ and the cargo-carrying motor densities, $u_1(\rho, t)$. We model the motor dynamics with advection diffusion equations coupled with switching terms to reflect delivery and uptake of vesicles to and from target sites. Let $c(\rho, t)$ denote the vesicle density at a distance ρ from the origin at time t. The system capturing the dynamics is

$$\frac{\partial u_0}{\partial t} = \frac{D}{\rho^2}\frac{\partial}{\partial \rho}\left(\rho^2 \frac{\partial u_0}{\partial \rho}\right) - \frac{\mathcal{V}_0}{\rho}\frac{\partial u_0}{\partial \rho} - \gamma_0 u_0 - k_+ c u_0 + k_- u_1 \tag{4.9a}$$

$$\frac{\partial u_1}{\partial t} = \frac{D}{\rho^2}\frac{\partial}{\partial \rho}\left(\rho^2 \frac{\partial u_1}{\partial \rho}\right) - \frac{\mathcal{V}_1}{\rho}\frac{\partial u_1}{\partial \rho} - \gamma_1 u_1 + k_+ c u_0 - k_- u_1 \tag{4.9b}$$

$$\frac{\partial c}{\partial t} = k_- u_1 - k_+ c u_0, \tag{4.9c}$$

where the various parameters are as in previous examples.. At steady state, we have the system,

$$D\frac{\partial^2 u_0}{\partial \rho^2} + \left(\frac{2D}{\rho} - \frac{\mathcal{V}_0}{\rho^2}\right)\frac{\partial u_0}{\partial \rho} - \gamma_0 u_0 = 0$$

$$D\frac{\partial^2 u_1}{\partial \rho^2} + \left(\frac{2D}{\rho} - \frac{\mathcal{V}_1}{\rho^2}\right)\frac{\partial u_1}{\partial \rho} - \gamma_1 u_1 = 0$$

$$c = \frac{k_- u_1}{k_+ u_0}.$$

Again, we obtain the steady state profiles numerically. Clearly, if $\mathcal{V}_1 = \mathcal{V}_0$, we have a uniform distribution of vesicles. When $\mathcal{V}_1 < \mathcal{V}_0$, we again have similar behavior to the 2D profiles, see figure 7. An explicit comparison of the distributions the 1D, 2D and 3D cases is shown in figure 8.

5. Discrete microtubule distributions

The models in section 4 were phenomenologically-based, under the assumption that we could treat a cytoskeletal network as a continuum, and model the effective motor transport as a radially symmetric advection-diffusion equation. It is possible to derive a higher-dimensional advection-diffusion equation from a more realistic stochastic model of 2D or 3D motor transport, in which individual motors switch between ballistic motion when bound to a microtubule and diffusive motion when unbound [2]. In general, the resulting advection-diffusion equation will be anisotropic, with an associated diffusion tensor that depends on the configuration of microtubules. Here we will consider a different regime in which the cytoskeletal network is sparse so that we have a discrete network. In order to simplify our analysis, we will assume that the microtubules project radially from the center of the disk or sphere. We can then derive an effective advection-diffusion equation for motor transport by following recent analysis of virus trafficking in cells [10, 16].

5.1. The disk

Consider a finite set of N identical, evenly spaced microtubules radiating from the center of the disk [10, 16]. That is, Ω_2 is partitioned into N equal slices, each of angular width $\Upsilon \equiv 2\pi/N$ (see figure 9), whose boundaries correspond to microtubules. Following Lawley *et al* [16], we will derive an effective advection-diffusion equation for motor transport by considering the dynamics of a single molecular motor moving within a single slice $\mathcal{U}_2 \equiv [\delta, \infty) \times [0, \Upsilon] \subset \Omega_2$—restriction to a single slice is allowed because of the symmetric partitioning and the fact that we are only interested in the radial distribution of motors.

Therefore, consider a single motor-cargo complex originating on ∂B_δ and undergoing Brownian motion in the interior of $\mathcal{U}_2$ until it reaches a microtubule, whence it binds to the microtubule and moves ballistically away from the origin for some exponentially distributed

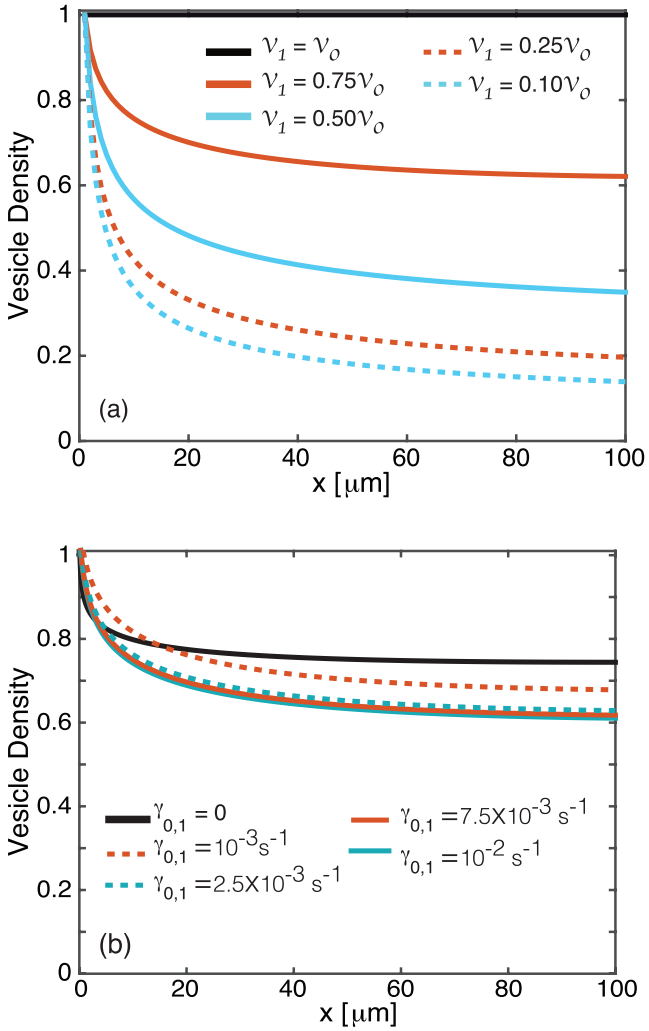

Figure 7. Figure depicting loss of uniform vesicle distribution on the sphere when $\mathcal{V}_1$ decreases. (a) Steady state distributions of vesicles in 3D sphere for various $\mathcal{V}_1$ values and fixed motor degradation rates $\gamma_{0,1} = 0.01\ s^{-1}$. (b) Corresponding plots for various degradation rates and $\mathcal{V}_1 = 0.75\ \mu m^3\ s^{-1}$. Other parameter values are as in figure 6.

amount of time. At this point the motor-cargo complex is reinserted into the slice at the current radius for some randomly selected angle between 0 and Υ. If $X(t)$ represents the motor's radial distance from the origin and $\theta(t)$ represents some angle between $[0, \Upsilon]$, the motor's motion is described by the following system of SDEs [10, 16]:

$$\mathrm{d}X = \begin{cases} V\,\mathrm{d}t & \theta = 0, \Upsilon \\ (D/X)\mathrm{d}t + \sqrt{2D}\,\mathrm{d}W_X & \theta \in (0, \Upsilon) \end{cases}$$
$$\mathrm{d}\theta = \begin{cases} 0 & \theta = 0, \Upsilon \\ (\sqrt{2D}/X)\mathrm{d}W_\theta & \theta \in (0, \Upsilon), \end{cases} \tag{5.1}$$

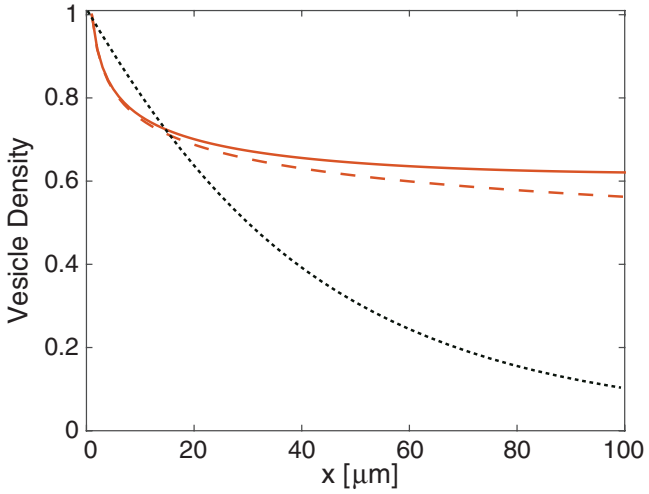

Figure 8. Comparison of profiles in 1D (dotted), 2D (dashed), and 3D (solid) domains for $v_1 = 0.075$ μm s^{-1} and $\mathcal{V}_1 = 0.75$ μm^2 s^{-1} for the disk and $\mathcal{V}_1 = 0.75$ μm^3 s^{-1} for the sphere. Other parameter values are as in figures 1 and 6.

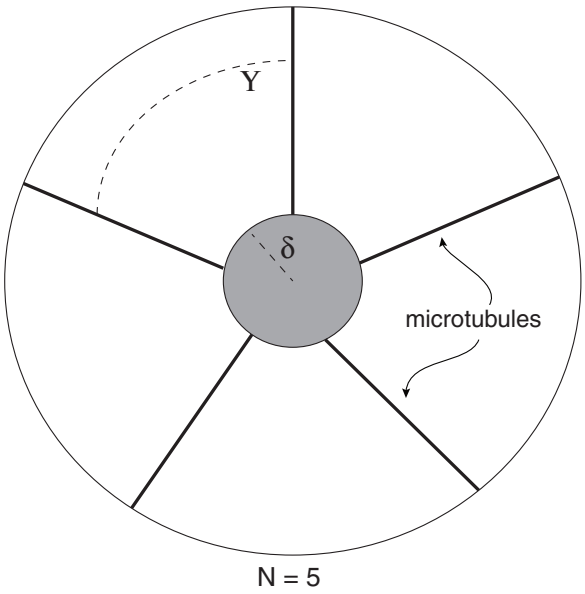

Figure 9. Partitioning of domain Ω_2 for $N = 5$.

where W_X, W_θ are standard independent Wiener processes, V is the motor velocity, and D is the motor diffusion coefficient. Note that one major difference from models of virus trafficking is that we are interested in the outward transport of motors from a source at the origin, whereas viruses enter the cell at some finite distance R from the cell center and move inwards in order to find the cell nucleus. In [16], Lawley *et al* use a coarse graining method to derive a single effective SDE describing the overall radial motion of a particle evolving according to equation (5.1). They assume there is a continuous-time jump Markov process underlying

the particle's switching between diffusive and ballistic dynamics, and that the dynamics of the Markov process are very fast relative to all other processes. Invoking an adiabatic (or quasi-steady state) approximation, they derive the following coarse-grained effective SDE approximation to equation (5.1):

$$\mathrm{d}X = \left(\frac{D}{X}\frac{T(X)}{\mu + T(X)} + V\frac{\mu}{\mu + T(X)}\right)\mathrm{d}t + \sqrt{2D\frac{T(X)}{\mu + T(X)}}\,\mathrm{d}W, \tag{5.2}$$

where $W(t)$ is a standard Wiener process, μ is the mean for the exponential distribution dictating the amount of time a particle spends in the ballistic phase, and $T(X)$ is the mean first passage time (MFPT) for a particle in the cytoplasm to reach a microtubule,

$$T(X) = \frac{\Upsilon^2 X^2}{12D}. \tag{5.3}$$

Let $p(r, t)$ represent the probability that a particle evolving according to equation (5.2) is at a distance r from the origin at time t. The corresponding Fokker–Planck equation is

$$\frac{\partial p}{\partial t} = -\frac{\partial}{\partial r}\left(\left[\frac{D}{r}\frac{T(r)}{\mu + T(r)} + V\frac{\mu}{\mu + T(r)}\right]p\right) + \frac{\partial^2}{\partial r^2}\left(D\frac{T(r)}{\mu + T(r)}p\right). \tag{5.4}$$

Now suppose that there are $\mathcal{N}$ independent motors evolving according to the SDE (5.2). Let $u(r, t)$ denote the density of motors at time t located a radial distance of r from the origin. We have the following relationship between $p(r, t)$ and $u(r, t)$:

$$p(r, t) = \frac{2\pi}{\mathcal{N}} r u(r, t), \tag{5.5}$$

where

$$\mathcal{N} = 2\pi \int_{\delta}^{\infty} r u(r, t)\mathrm{d}r.$$

We are assuming that u decays sufficiently fast at infinity. Substituting equations (5.5) into (5.4) yields the following PDE for motor density dynamics:

$$\frac{\partial u}{\partial t} = -\frac{1}{r}\frac{\partial}{\partial r}\left(\left[D\frac{T(r)}{\mu + T(r)} + Vr\frac{\mu}{\mu + T(r)}\right]u\right) + \frac{1}{r}\frac{\partial^2}{\partial r^2}\left(D\frac{T(r)}{\mu + T(r)}ru\right) \tag{5.6}$$

Using equation (5.6) as a starting point, we now investigate reversible vesicle delivery for the discrete microtubule set case.

Consider the dynamics of free motors with density $u_0(r,t)$ and cargo-carrying motors with density $u_1(r,t)$. Each evolves according to an equation of the form (5.6), coupled with switching terms that reflect vesicle delivery and uptake. Again, let $c(r,t)$ denote the vesicle density at a distance r from the origin at time t. The system of equations is then

$$\frac{\partial u_0}{\partial t} = -\frac{1}{r}\frac{\partial}{\partial r}\left(\left[D\frac{T(r)}{\mu + T(r)} + V_0 r\frac{\mu}{\mu + T(r)}\right]u_0\right) + \frac{1}{r}\frac{\partial^2}{\partial r^2}\left(D\frac{T(r)}{\mu + T(r)}ru_0\right) - k_+ c u_0 + k_- u_1 \tag{5.7a}$$

$$\frac{\partial u_1}{\partial t} = -\frac{1}{r}\frac{\partial}{\partial r}\left(\left[D\frac{T(r)}{\mu + T(r)} + V_1 r\frac{\mu}{\mu + T(r)}\right]u_1\right) + \frac{1}{r}\frac{\partial^2}{\partial r^2}\left(D\frac{T(r)}{\mu + T(r)}ru_1\right) + k_+ c u_0 - k_- u_1 \tag{5.7b}$$

$$\frac{\partial c}{\partial t} = k_- u_1 - k_+ c u_0, \tag{5.7c}$$

with D, $V_{0,1}$, $k_\pm$ defined as in previous cases. One important difference is that we no longer include motor degradation terms, since these would lead to a breakdown of the analysis of Lawley *et al* [16]. However, as shown in the continuum case, the profiles are relatively insesiitive to the degradation rate, see figures 6(b) and 7(b). Again we find that a uniform steady-state distribution of vesicles occurs when $V_0 = V_1$, but there is a loss in uniformity when $V_1 < V_0$. This is illustrated in figure 10(a) where we show numerical plots of the steady-state solutions.

5.2. Sphere

Let Ω_3 be defined as in section 4.2, but now we let the set of microtubules emanating from the origin be discrete rather than a continuum, see figure 11. Hence, we have a natural partition for $\Omega_3 = \omega_1 \cup \omega_2$. We define ω_1 in the following way. Let N be the number of microtubules emanating out from the small sphere of radius δ enveloping the origin. These can be modeled as infinite cylinders each of radius ε. Let $\mathbf{c}_i$ for $i = 1...N$ denote a randomly selected fixed position on the δ-sphere. Then each microtubule $\mathcal{M}_i$ is defined as follows:

$$\mathcal{M}_i \equiv \{\mathbf{x} \in \Omega_3 \big| \|\mathbf{x} - \rho \mathbf{c}_i\| \leqslant \varepsilon, \rho \in [\delta, \infty)\}.$$

We take $\omega_1 = \cup_{i=1}^N \mathcal{M}_i$ and $\omega_2 = \Omega_3 \setminus \omega_1$. To model the dynamics of motor-cargo complexes in this domain, we must derive PDEs from the SDEs describing the motion of a single particle in this domain. We assume a single particle's motion is characterized by standard Brownian motion in ω_2 until it reaches a microtubule, when it undergoes ballistic motion with fixed velocity V away from the origin for some exponentially distributed time. The particle is then released at a random position in Ω_3 with radius equal to how far it reached with ballistic motion. Lawley *et al* provide the following SDE as a coarse-grain approximation to a particle moving through Ω_3 as described above:

$$\mathrm{d}X = \left(\frac{2D}{X} \frac{T(X)}{\mu + T(X)} + V \frac{\mu}{\mu + T(X)} \right) \mathrm{d}t + \sqrt{2D \frac{T(X)}{\mu + T(X)}}\, \mathrm{d}W, \tag{5.8}$$

where $X(t)$ is the distance of a particle from the origin, D is the diffusion coefficient, V is the particle velocity, $W(t)$ is a Wiener process, μ is the mean for the exponential density for the amount of time a particle spends on a microtubule, and $T(X)$ is the MFPT for a particle beginning at position X to reach a microtubule. Coombs, Straube, and Ward provide the following asymptotic approximation for $T(X)$ in the small ε limit:

$$T(X) = \frac{X^2}{D}\left[-\frac{2}{N} \ln\left(\frac{\varepsilon}{X}\right) + \ln 4 - 1 - \frac{4}{N^2}\Psi \right]$$

with

$$\Psi = \sum_{k=1}^{N} \sum_{j=k+1}^{N} \ln\|\mathbf{c}_k - \mathbf{c}_j\|$$

Let $p(\rho, t)$ represent the probability that a particle is at position ρ at time t. The Fokker–Planck equation associated with equation (5.8) is

$$\frac{\partial p}{\partial t} = -\frac{\partial}{\partial \rho}\left[\left(\frac{2D}{\rho} \frac{T(\rho)}{\mu + T(\rho)} + V \frac{\mu}{\mu + T(\rho)} \right) p \right] + D \frac{\partial^2}{\partial \rho^2}\left(\frac{T(\rho)}{\mu + T(\rho)} p \right) \tag{5.9}$$

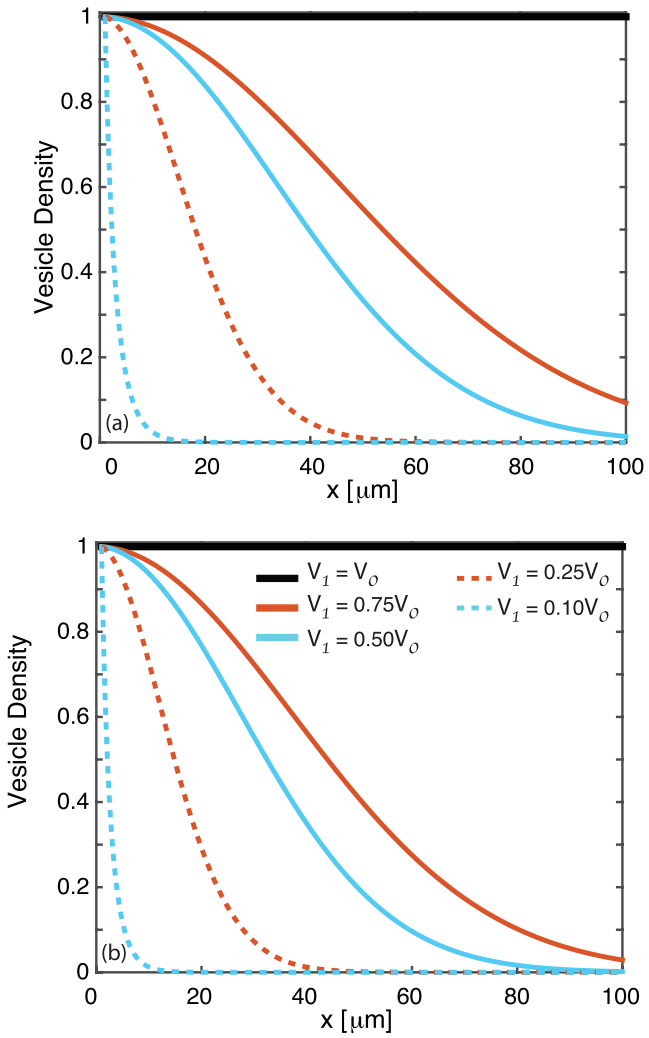

Figure 10. Figure showing the loss of vesicle uniformity for $V_1 < V_0 = 1$ and discrete distribution of microtubules. (a) The disk with $N = 12$ microtubules. (b) The sphere with $N = 1000$ microtubules. Other parameter values are $D = 0.1\ \mu\text{m}^2\ \text{s}^{-1}$, $\delta = 0.1\ \mu\text{m}$, $k_\pm = 0.01\ \text{s}^{-1}$, $u_0^0 = u_1^0$.

Now suppose that there are $\mathcal{N}_S$ independent motors evolving according to equation (5.8). If $u(\rho, t)$ denotes motor density at a distance ρ from the origin at time t, we have the following relation between $p(\rho, t)$ and $u(\rho, t)$

$$p(\rho, t) = \frac{4\pi}{\mathcal{N}_S}\rho^2 u(\rho, t) \tag{5.10}$$

where

$$\mathcal{N}_S = 4\pi \int_\delta^\infty \rho^2 u(\rho, t)\mathrm{d}\rho$$

Substituting equations (5.10) into (5.9) gives

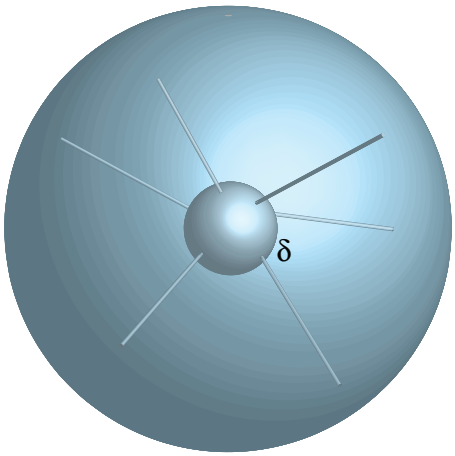

Figure 11. Sketch of Ω_3 showing $N = 6$ microtubules radiating from center.

$$\frac{\partial u}{\partial t} = -\frac{1}{\rho^2}\frac{\partial}{\partial \rho}\left[\left(2D\rho\frac{T(\rho)}{\mu + T(\rho)} + V\rho^2\frac{\mu}{\mu + T(\rho)}\right)u\right] + \frac{D}{\rho^2}\frac{\partial^2}{\partial \rho^2}\left(\frac{T(\rho)}{\mu + T(\rho)}\rho^2 u\right) \tag{5.11}$$

Equation (5.11) is the PDE describing the dynamics of motor density in Ω_3. We now use it as the governing PDE to investigate reversible vesicular delivery in a sphere.

Consider the dynamics of free motors with density $u_0(r,t)$ and cargo-carrying motors with density $u_1(r,t)$. Each evolves according to an equation of the form (5.6), coupled with switching terms that reflect vesicle delivery and uptake. Again, let $c(r,t)$ denote the vesicle density at a distance r from the origin at time t. The system of equations is then

$$\frac{\partial u_0}{\partial t} = -\frac{1}{\rho^2}\frac{\partial}{\partial \rho}\left[\left(2D\rho\frac{T(\rho)}{\mu + T(\rho)} + V_0\rho^2\frac{\mu}{\mu + T(\rho)}\right)u_0\right] + \frac{D}{\rho^2}\frac{\partial^2}{\partial \rho^2}\left(\frac{T(\rho)}{\mu + T(\rho)}\rho^2 u_0\right) - k_- c u_0 + k_+ u_1 \tag{5.12a}$$

$$\frac{\partial u_1}{\partial t} = -\frac{1}{\rho^2}\frac{\partial}{\partial \rho}\left[\left(2D\rho\frac{T(\rho)}{\mu + T(\rho)} + V_1\rho^2\frac{\mu}{\mu + T(\rho)}\right)u_1\right] + \frac{D}{\rho^2}\frac{\partial^2}{\partial \rho^2}\left(\frac{T(\rho)}{\mu + T(\rho)}\rho^2 u_1\right) + k_- c u_0 - k_+ u_1 \tag{5.12b}$$

$$\frac{\partial c}{\partial t} = k_+ u_1 - k_- c u_0 \tag{5.12c}$$

Again we find that a uniform steady-state distribution of vesicles occurs when $V_0 = V_1$, but there is a loss in uniformity when $V_1 < V_0$. This is illustrated in figure 10(b) where we show numerical plots of the steady-state solutions.

6. Discussion

In this paper, we investigated a possible biophysical mechanism for facilitating a more uniform distribution of vesicles to targets dispersed throughout cells of various geometries. In particular, we generalized the results found in [4] by examining the impact of allowing for reversibility in vesicular delivery to target sites on a Cayley tree, a disk, and a sphere. On the disk and sphere, we considered both a continuous distribution of microtubules and a discrete

set. In the latter case, we derived an effective advection-diffusion equation for motor transport based on SDEs for single motor motion, following along similar lines to [16]. In all cases, we found that uniformity in the steady state-vesicle distribution is attainable if vesicle delivery is reversible, and the velocity of cargo-carrying motors is not significantly less than that of free motors. We also characterized the loss of uniformity when there was a mismatch between the velocities of free and cargo-bound motors.

There are a number of issues we wish to explore in future work. In this paper, we assumed each motor carried only one cargo element. It would be interesting to relax this condition and allow each motor to carry a collection of cargo elements that can be delivered to target sites. This problem was previously investigated for a 1D track using aggregation theory and a modified version of the Becker–Doring equations in [5]. A related problem is developing a more detailed model of bidirectional motor transport. This is particularly important in determining how the effective speed of a motor-cargo complex depends on the cargo load, for in order to a achieve a more uniform distribution of resources using the proposed mechanism, it is necessary that the speed is weakly dependent on cargo load. In the case of large vesicles, this would require that transport involves cooperation between multiple molecular motors, rather than a single motor. There is considerable debate in the literature regarding the most likely mechanism for cooperative bidirectional transport [7, 14, 20]: (a) an asymmetric tug-of war model involving the joint action of multiple kinesin and dynein motors pulling in opposite directions; (b) a symmetric tug-of-war model where all the motors are of the same type, but they are distributed on microtubules of opposite polarity; (c) a hopping model, in which the whole motor-cargo complex hops between microtubules of opposite polarity; (d) some form of coordination complex that controls the switching between different motor species. Yet another related issue is developing a more detailed model of the exchange of vesicular cargo between motors and targets. In this paper, we simply took the exchange to be given by first-order kinetics, and assumed that there was a uniform distribution of targets throughout the cell. The latter is likely to be a particularly crude approximation in the case of higher-dimensional cell geometries. For example, in the case of discrete microtubular networks, one might expect targets to be located within some local neighborhood of the microtubules.

A natural extension of the analysis on a tree would be to take successive generations of the tree to have different properties, reflecting the fact that in axons (and dendrites) the branches tend to taper off (become thinner). A further generalization of this work would be to account for exclusion effects between motor-cargo complexes. We previously investigated the impact of exclusion effects on steady-state vesicle densities on a 1D track in [6], and asymmetric exclusion processes have been studied on a Cayley tree [1, 19]. Another interesting problem is how one would extend the analysis of Lawley *et al* [16] to more general configurations of microtubules. One of the essential steps in their analysis is the adiabatic approximation that during the time between binding and unbinding to a microtubule the relative change in radial position is small. This has several implications for our own analysis. First, the adiabatic approximation breaks down at sufficiently large radii, as can be seen from the formula for the MFPT in equation (5.3), that is, $T(X) \sim X^2$. Thus, a more careful analysis would need to restrict the dynamics to a bounded domain and take the number of microtubules to be sufficiently large. The adiabatic requirement also meant that we had to neglect the degradation of motor-cargo complexes. Again, it would be interesting to extend the analysis of [16] to allow for the possibility that motors disappear so that one has to determine a conditional MFPT.

Finally, we hope to investigate other biological processes involving motor transport on interesting geometries. For example, we recently developed a mathematical model of a molecular motor-based axonal length sensing mechanism using delay differential equations and

advection-diffusion PDEs [12] on a 1D domain, but a more realistic model would account for axonal branching. Hence, a Cayley tree geometry may be more appropriate as a domain.

Acknowledgments

PCB was supported by the National Science Foundation (DMS-1613048).

References

[1] Basu M and Mohanty P K 2010 Asymmetric simple exclusion process on a Cayley tree *J. Stat. Mech.* P10014
[2] Bressloff P C and Newby J M 2011 Quasi-steady state analysis of motor-driven transport on a two-dimensional microtubular network *Phys. Rev.* E **83** 061139
[3] Bressloff P C 2014 *Stochastic Processes in Cell Biology* (Berlin: Springer)
[4] Bressloff P C and Levien E 2015 Synaptic democracy and active intracellular transport in axons *Phys. Rev. Lett.* **114** 168101
[5] Bressloff P C 2016 Aggregation-fragmentation model of vesicular transport in neurons *J. Phys. A: Math. Theor.* **49** 145601
[6] Bressloff P C and Karamched B R 2016 Model of reversible vesicular transport with exclusion *J. Phys. A: Math. Theor.* **49** 345602
[7] Gross S P 2004 Hither and Yon: a review of bi-directional microtubule-based transport *Phys. Biol.* **1** R1-11
[8] Hoerndli F J, Maxfield D A, Brockie P J, Mellem J E, Jensen E, Wang R, Madsen D M and Maricq A V 2013 Kinesin-1 regulates synaptic strength by mediating the delivery, removal, and redistribution of AMPA receptors *Neuron* **80** 1421–37
[9] Huber F, Schnauss J, Ronicke S, Rauch P, Muller K, Futterer C and Kas J 2013 Emergent complexity of the cytoskeleton: from single filaments to tissue *Adv. Phys.* **62** 1–112
[10] Lagache T and Holcman D 2008 Effective motion of a virus trafficking inside a biological cell *SIAM J. Appl. Math.* **68** 1146–67
[11] Howard J 2001 *Mechanics of Motor Proteins and the Cytoskeleton* (Sunderland: Sinauer)
[12] Karamched B R and Bressloff P C 2015 A delayed feedback model of axonal length sensing *Biophys. J.* **108** 240819
[13] Keren K, Pincus Z, Allen G M, Barnhart E L, Marriott G, Mogilner A and Theriot J A 2008 Mechanism of shape determination in motile cells *Nature* **453** 475–80
[14] Kural C, Kim H, Syed S, Goshima G, Gelfand V I and Selvin P R 2005 Kinesin and dynein move a peroxisome *in vivo*: a tug-of-war or coordinated movement? *Science* **308** 1469–72
[15] Lemieux M, Labrecque S, Tardif C, Labrie-Dion E, LeBel E and De Koninck P 2012 Translocation of CaMKII to dendritic microtubules supports the plasticity of local synapses *J. Cell Biol.* **198** 1055–73
[16] Lawley S D, Tuft M and Brooks H A 2015 Coarse-graining intermittent intracellular transport: two- and three-dimensional models *Phys. Rev.* E **92** 042709
[17] Maeder C I, San-Miguel A, Wu E Y, Lu H and Shen K 2014 *In vivo* neuron-wide analysis of synaptic vesicle precursor trafficking *Traffic* **15** 273–91
[18] Maree A F, Jilkine A, Dawes A, Grieneisen V A and Edelstein-Keshet L 2006 Polarization and movement of keratocytes: a multiscale modelling approach *Bull. Math. Biol.* **68** 1169–211
[19] Mottishaw P, Waclaw B and Evans M R 2013 An exclusion process on a tree with constant aggregate hopping rate *J. Phys. A: Math. Theor.* **46** 405003
[20] Muller M J I, Klumpp S and Lipowsky R 2008 Tug-of-war as a cooperative mechanism for bidirectional cargo transport by molecular motors *Proc. Natl Acad. Sci. USA* **105** 4609–14
[21] Newby J M and Bressloff P C 2009 Directed intermittent search for a hidden target on a dendritic tree *Phys. Rev.* E **80** 021913
[22] Newby J M and Bressloff P C 2010 Quasi-steady state reduction of molecular motor-based models of directed intermittent search *Bull. Math. Biol.* **72** 1840–66

[23] Settembre C, Fraldi A, Medina D L and Ballabio A 2013 Signals from the lysosome: a control centre for cellular clearance and energy metabolism *Nat. Rev. Mol. Cell Biol.* **14** 283–96
[24] Waites C L, Craig A M and Garner C C 2005 Mechanisms of vertebrate synaptogenesisa *Annu. Rev. Neurosci.* **28** 251–74
[25] Wong M Y, Zhou C, Shakiryanova D, Lloyd T E, Deitcher D L and Levitan E S 2012 Neuropeptide delivery to synapses by long-range vesicle circulation and sporadic capture *Cell* **148** 1029–38